



Predictive energy-saving optimization based on nonlinear model predictive control for cooperative connected vehicles platoon with V2V communication

Fangwu Ma ^{a,1}, Yu Yang ^{a,*¹,1}, Jiawei Wang ^a, Zhenze Liu ^b, Jinhang Li ^a, Jiahong Nie ^a, Yucheng Shen ^a, Liang Wu ^{a,**}

^a State Key Laboratory of Automotive Simulation and Control, Jilin University 5988, Renmin Ave., Changchun, 130025, China

^b College of Communication Engineering, Jilin University 5988, Renmin Ave., Changchun, 130025, China

ARTICLE INFO

Article history:

Received 24 January 2019

Received in revised form

31 July 2019

Accepted 11 September 2019

Available online 17 September 2019

Keywords:

Energy consumption

Ecological cooperative adaptive cruise

control (eCACC)

Model predictive control

Vehicles platoon

V2V communication

ABSTRACT

The rise of the intelligent transportation system (ITS) brings golden opportunity to accelerate the development of environment-friendly smart mobility eco-system. The intelligent control of connected autonomous vehicles (CAV) platoon with V2V communication as the core technology exhibits superior energy-saving potential. However, there still exist plentiful technologies of the emerging vehicle platoon need to be improved. Hence, this paper describes a predictive optimization strategy as ecological cooperative adaptive cruise control (eCACC) based on nonlinear model predictive control (NMPC) to minimize the energy consumption of an electrified CAV platoon considering V2V topological communication structure of leader predecessor follower. The cost function for NMPC includes the following velocity, range deviation and energy consumption. Through the simulation analysis under various drive cycles, the advantage of the proposed scheme emerges that the platoon consisted of three vehicles possesses the nice string stability, excellent following performance and significant energy-saving potential at same time. Moreover, the acceleration of the following vehicles is in a small range, improving the drive comfort. By the comparison with the existed Eco ACC controller, the simulation results demonstrate the proposed controller owns better following performance and energy-saving behavior of 16.1%, 6.2% and 11.7% under full UDDS, HWFET and NEDC drive cycle, respectively.

© 2019 Elsevier Ltd. All rights reserved.

1. Introduction

The increasingly serious environmental pollution poses a series of new challenges to automotive technology to build a clean and efficient mobility ecosystem [1–3]. Therefore, a plenty of energy-saving approaches are widely investigated and applied, such as high efficiency internal combustion engine [4], alternative clean energy [5,6], eco-driving technology [7,8], etc. Among multitudinous energy economy technology routes, electric vehicles obtain much approval and promotion of many scholars worldwide based on the features of eco-friendly and huge energy saving potential [9–11]. In the meantime, with the rapid development of Intelligent

Transportation System (ITS) and connected autonomous vehicles (CAV), eco-driving technology is developed in a new stage. ITS could help to shorten the actual intervehicle range, increase the traffic flow per unit time and solve the problem of traffic congestion, resulting in reduce energy consumption of the whole system by upper-layer traffic flow control [12,13]. With the gradual enhancement of the vehicle connectivity and intellectualization, CAV has better performance to response the traffic dispatching of ITS and achieve highly autonomous driving, avoiding the adverse human-drive habits such as rapid acceleration and deceleration. Hence, that accomplishes the purpose of energy-saving by utilizing the advanced bottom-layer powertrain control [14].

Eco-driving as one of the core technologies of ITS attracts much attention from researchers who make plentiful contributions in such fields [3,15–18]. Fredette et al. compared three representative method included Ad-Hoc, Hamilton-Jacobi and Dynamic Programming to explore the fuel saving performance in complicated traffic condition [19]. Thibault et al. extended the endurance

* Corresponding author.

** Corresponding author.

E-mail addresses: yyu0821@163.com (Y. Yang), astdwxg@jlu.edu.cn (L. Wu).

¹ F. Ma and Y. Yang equally contributed to this research work.

mileage of electric vehicles by eco-routing with the identification of traffic condition and subsequent real-time optimal speed profile advising to the driver [20]. Many researchers take advantage of connectivity of ITS to achieve eco-approach and departure at signalized intersection, which makes benefits for energy economy and drive comfort [8,21,22]. Moreover, the advanced bottom-layer control strategy for a single vehicle also presents the excellent energy-saving potential. Qi et al. suggested a co-optimization strategy of both vehicle dynamics and powertrain for plug-in hybrid electrical vehicle by using the real-world data, which exhibits 24% fuel saving in the urban flow condition [13]. Lei et al. designed a novel electric powertrain for electric vehicle using in-wheel motor with low energy consumption potential [23].

With the gradual maturity of communication technology in the recent years, vehicle-vehicle and vehicle-infrastructure cooperative technologies greatly respond to the call for building an environmentally friendly society. Therefore, the multi-vehicle cooperative control on various significative purpose as a hot research topic was investigated in an increasing number. Among these researches, the representative control algorithms and objectives were selected in Table 1, where exhibits a more understandable and comprehensive comparation. Internal combustion engine vehicle (ICEV) as the most-used driving choices till now was widely investigated in the platooning forms to explore further performance which could be applied in the ITS. Wang et al. preliminarily explored the platoon driving performance focusing on car-following mode consisting of two ICEVs using MPC algorithm and obtained the results of car-following and energy consumption situation under the drive cycles where although the performance needs to be improved, the plenty of works still provide a significative reference to the future research [24]. Orosz et al. used nonlinear, multi-input, proportional integral-velocity-acceleration (PIVA) controller to optimize the car-following performance with consideration of time delay influencing connected cruise control (CCC) [25]. Besides, there also exists some novel driving mode like Pulse and Glide (PnG) proposed by Li et al. who mainly utilized Periodic Switching Control (PSC) to the ICEV platoon and achieved excellent results of energy saving [14]. Except for ICEV, the plug-in hybrid electric vehicle (PHEV) also attracted much attention to improve their car following performance and energy economy especially in the mode of adaptive cruise control such as the works investigated by Vajedi et al. where the followed vehicle with eco-ACC controller using NMPC shows favorable simulation results [26]. With the gradual maturity of communication technology especially the coming 5G communication, vehicle-vehicle and vehicle-infrastructure cooperative technologies could well satisfy the high requirements of ITS. Therefore, a more promising control mode called cooperative adaptive cruise control (CACC) for vehicle platoon gradually comes to consideration of researchers. The basic of CACC is the stability of platoon and some researchers focus on this area like that Zheng et al. proposed decentralized asymmetric control (DAC) to investigate the stability under undirected communication topologies of platoon and obtain the superior performance [27]. Hu et al. proposed a look-ahead model predictive control to optimize the

efficiency of engine and CVT with V2V communication, which decreases the fuel consumption meanwhile ensure the safe following performance of the followed vehicle [28]. Zhai et al. increased the fuel economy of the vehicle platoon using distributed model predictive control and evaluated the comprehensive properties on road slopes [29]. Li et al. combines the advantages of hybrid electric vehicles and smart vehicles to improve the fuel economy, safety and comfort at same time during a car-following process and prove the lower fuel consumption compare to the implement of adaptive cruise control with energy management strategy [30]. However, the above plentiful works focus on energy-saving strategy of single traditional petrol vehicle and car following process by no more than two vehicles with a limited following performance. Very few publications investigate the energy-saving potential of fully electric vehicle platoon consisted of more than two vehicles with communication topology. Moreover, due to the appeal for eco intelligent transportation system, electric vehicles become mainstream and will be developed towards more mini-sized, sustainable and flexible to satisfy the human's daily travel requirements.

Herein, this paper took a step forward on the basis on the string stability and proposed ecological cooperative adaptive cruise control (eCACC) combining with both car-following performance and energy consumption for the mini electric vehicles (mini-EV) platoon under the consideration of LPF communication topology. The predictive energy-saving strategy using nonlinear model predictive control was proposed for a CAV platoon consisted of three electric vehicles with V2V topological communication structure of leader predecessor follower (LPF), which demonstrates excellent following performance and energy economy at same time. The essence of the proposed NMPC strategy is a predictive multi-objective optimization considering the following velocity, range deviation and energy consumption with weight coefficient. Moreover, the proposed scheme was evaluated in the urban and highway drive cycle by analyzing the longitudinal dynamics of the platoon and the operating parameters such as acceleration, motor efficiency of the two following vehicles. The simulation result of the two following vehicles indicates that the platoon exhibits a nice string stability when speed variation regarded as low frequency disturbance occurs in the leading vehicle. The fluctuation of the following vehicles is convergent. Further, the proposed scheme is compared with an existing eco ACC controller, revealing the preferable following performance and less energy consumption of 16.1%, 6.2% and 11.7% under full UDDS, HWFET and NEDC drive cycle, respectively.

The rest of this paper is organized as follows. Section 2 provides the system dynamics modeling included longitudinal dynamics model of the vehicle platoon and dynamics model of single electric vehicle with in-wheel motors. Section 3 describes the integrated energy-saving NMPC strategy. The performance evaluation of the proposed scheme under various drive cycle is carried out in Section 4. While the comparation with the eco-ACC controller is presented in Section 5. Subsequently, the paper is summarized and comes to a conclusion in Section 6.

Table 1
Overview of the current researches about multi-vehicle control.

Vehicle	Control Algorithm	Optimization Objective	Cruise Mode	Ref.
ICEV	MPC	Car-following performance + Energy consumption	Car-following	24
ICEV	PIVA	Time Delay	CCC	25
ICEV	PSC	Energy consumption	PnG	14
PHEV	NMPC	Car-following performance + Energy cost	Eco-ACC	26
N/A	DAC	Stability under Undirected Topologies	CACC	27
MEV	NMPC	Car-following performance + Energy consumption	eCACC	This work

2. System dynamics modeling

Fig. 1 describes the schematic illustration of investigated CAV platoon which is consisted of the fully mini electric vehicles with the same parameters using V2V connectivity. The topological communication structure of LPF is utilized, referring to that the following vehicle receive the information both from the preceding vehicle and leading vehicle. The headway gap is introduced here to improve the string stability of the platoon [25].

2.1. Discrete longitudinal dynamics model

The time-based discrete longitudinal dynamics model is established by the Newton's second law, which is shown as

$$\begin{cases} s_n(k+1) = s_n(k) + v_n(k)\delta t \\ v_n(k+1) = v_n(k) + a_n(k)\delta t \\ a_n(k) = -\frac{C_{n,D}\rho_n A_n v_n^2(k)}{2m} - g(\mu \cos(\theta) + \sin(\theta)) + u_n(k) \\ \delta h(k) = h_d(k) - h_c(k) \\ h_d(k) = \tau_h v_n(k) + r_0 + l_0 \\ h_c(k) = s_{n-1}(k) - s_n(k) \end{cases} \quad (1)$$

where $s_n(k)$ is position of the n th vehicle at k time point. Similarly, $v_n(k)$, $a_n(k)$ refers to the velocity and acceleration. δt indicates the discrete time interval and $C_{n,D}$, ρ_n , A_n , m are the air drag factor, air density, frontal area and mass of the vehicle n , respectively. g , μ and θ represent the acceleration of gravity, coefficient of ground friction and angle of gradient. $u_n(k)$ is regarded as specific traction which will be the control variable in the following context. The deviation of intervehicle range $\delta h(k)$ between two vehicles is regarded as a core factor influencing the string stability. In this case, the desirable headway $h_n(k)$ between mass center of two vehicles can be defined as that the velocity difference of the two vehicles multiply headway time τ_h and plus the length of the vehicle l_0 and the minimum initial safe intervehicle distance r_0 referring to the assigned range when the velocity of both vehicles equals to zero. The current intervehicle range is expressed as $h_c(k)$.

2.2. In-wheel motor dynamic model

Here, the vehicles are rear wheel driven by two permanent magnet synchronous in-wheel motors (PMSM), the simplified dynamic model of which is established as the following

$$F_{n,x}(k)r_w = T_{n,x}(k) - J_{n,x} \frac{\omega_{n,x}(k+1) - \omega_{n,x}(k)}{\delta t} \quad (2)$$

where parameters $F_{n,x}(k)$, $T_{n,x}(k)$, $\omega_{n,x}(k)$ are the traction force, torque and rotate speed of in-wheel motor x . Due to the mechanical structure of the motor and wheel, $J_{n,x}$ is defined as the combined

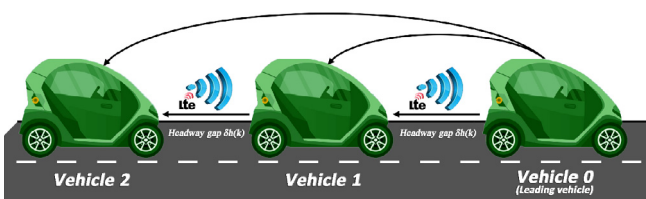


Fig. 1. Schematic illustration of CAV platoon driving with V2V communication.

rotary inertia.

At the same time, the rotate speed $\omega_{n,x}(k)$ is also involved with vehicle velocity, wheel side gear ratio g_n and the wheel radius r_w , describing as:

$$\omega_{n,x}(k) = \frac{60v_n(k)g_n}{2\pi r_w} \quad (3)$$

The maximum out-put driving traction of the in-wheel motor is provided by the ground friction influencing by the normal load of driving wheel which refers to the rear ones. The normal load of the rear wheel could be exhibited as

$$F_{r,x}(k) = \frac{g}{L_n} (0.5L_n \cos(\theta, k) + H_n \sin(\theta, k)) + \frac{mH_n}{L_n} \left(\frac{v_n(k+1) - v_n(k)}{\delta t} \right) \quad (4)$$

where L_n is the wheel base and H_n is the height of mass center of the vehicle. Here, the front and rear axle distance from center of gravity are assumed as the same value to reduce computation and simplify complexity. The vehicle platoon is considered in longitudinal dynamic driving on flat road ($\theta = 0$, $\cos(\theta, k) = 0$, $\sin(\theta, k) = 1$) without steering motion, resulting in the 2 rear in-wheel motors perform the same normal force which could be simplified as

$$F_{r,x}(k) = \frac{mH_n}{L_n} \left(\frac{v_n(k+1) - v_n(k)}{\delta t} \right) + 0.5g \quad (5)$$

The maximum traction torque is constrained as

$$T_{n,x}(k) = \mu F_{r,x}(k) r_w \quad (6)$$

2.3. Thevenin model of battery

As is shown in **Fig. 2**, the Thevenin model of battery is used to exhibit the excellent dynamics characteristic while it possesses the first-order which is beneficial for engineering implementation [31]. According to Kirchhoff's first law, the electrical performance of the circuit is deduced as

$$\begin{cases} V(k) = V_{OC}(k) - V_s(k) - I(k)R_e(k) \\ \dot{V}_s(k) = -\frac{V_s(k)}{R_s(k)C_s(k)} + \frac{I(k)}{C_s(k)} \end{cases} \quad (7)$$

where $V(k)$, $V_{OC}(k)$ are the terminal voltage and open circuit voltage of the battery. $V_s(k)$ represents the voltage of the polarization

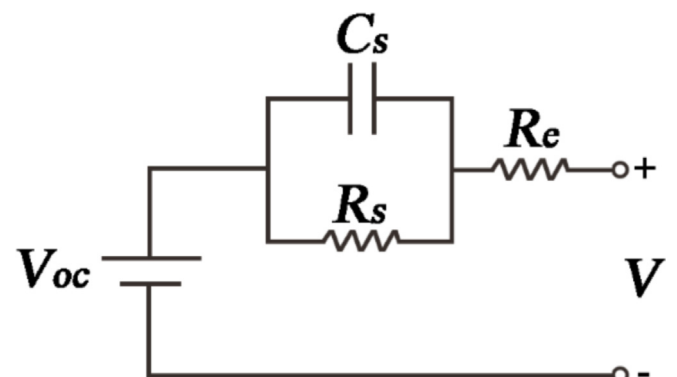


Fig. 2. Battery equivalent circuit model (first-order RC model).

resistance $R_s(k)$. Parameter $C_s(k)$ is the equivalent capacitance and $R_e(k)$ denotes ohmic resistance of battery as well as $I(k)$ is the charge/discharge current.

The terminal power $P(k)$ is as the following,

$$P(k) = (V_{OC}(k) + V_s(k))I(k) - I^2(k)R_e(k) \quad (8)$$

Accordingly, the SOC (state of charge) of the battery in the time-based discrete version is defined as

$$SOC(k+1) = SOC(k) - \frac{I(k)\delta t}{Q_{MAX}} \quad (9)$$

where Q_{MAX} is the total battery capacity.

Substituting the expression of $I(k)$ into formula (9), the SOC can be rewrites in the following form:

$$SOC(k+1) = SOC(k) - \frac{(V_{OC}(k) + V_s(k)) - \sqrt{(V_{OC}(k) + V_s(k))^2 - 4R_e(k)T_{n,x}(k)\omega_{n,x}(k)\eta_m(k)\eta_b(k)^{-\text{sgn}(T_m(k))}}}{2R_e(k)Q_{MAX}} \delta t \quad (10)$$

where η_m , η_b are the efficient of the in-wheel motor and battery pack.

2.4. Energy consumption model

For fully electric vehicles, the energy efficient does mainly on the operating status of the in-wheel motors, which means that torque and rotate speed need located in the high efficiency region. Moreover, the ability of regenerative braking energy needs to be improved when the vehicle is in braking situation refers to the negative torque [9]. However, that does not mean that more braking force will be beneficial to reduce energy consumption. After all, the energy is conserved, and energy will be loss while involved in energy conversion. Therefore, decreasing unnecessary energy conversion can make contribution to energy saving. The energy consumption model can be described as:

$$q_n(k) = \begin{cases} \sum_{x=1}^2 \frac{P_{out_x}\delta t}{\eta_m(T_{n,x}(k), \omega_{n,x}(k))\eta_b} & a_n(k) > 0 \\ \sum_{x=1}^2 -P_{in_x}\eta_m(T_{n,x}(k), \omega_{n,x}(k))\eta_b\delta t & a_n(k) \leq 0 \end{cases} \quad (11)$$

$$\dot{SOC}_n = - \frac{(V_{OC}(k) + V_s(k)) - \sqrt{(V_{OC}(k) + V_s(k))^2 - 4R_e(k)T_{n,x}(k)\omega_{n,x}(k)\eta_m(k)\eta_b(k)^{-\text{sgn}(T_m(k))}}}{2R_e(k)Q_{MAX}} \quad (13)$$

where $q_n(k)$ is the energy consumption of n th vehicle at k point. Parameters P_{out_x} , represent the output power while acceleration $a_n(k)$ is positive and P_{in_x} is input power while $a_n(k)$ is negative of the in-wheel motor x .

3. Predictive energy-saving strategy based on NMPC

In the vehicle-following model, the leading vehicle delivers its state parameters to the other vehicles of the intelligent connected vehicle platoon using V2V communication, where the influence of communication delay and packet dropout are not under the consideration. As for the communication topology of the platoon, a high string stable structure that following vehicles receive the signals from their preceding vehicles and the leading vehicle with the equal weight factor is utilized [32,33].

In order to optimize the energy efficiency of the platoon, the favorable vehicle-following performance is the key prerequisite. Here, a nonlinear model predictive control (NMPC) is proposed to cover the above issue. Moreover, the above description belongs to nonlinear process, resulting in a strong requirement of computing ability. Therefore, the whole process is discretized in 0.1 s, which

could efficiently predict the output of the system at time step $k+1$ using the system state and control variables input at point k . In this case, the input at time k is used to control the output of the system at time $k+1$, so that it is as close as possible to the expected value at time $k+1$ [34].

In this paper, the longitudinal dynamics of the vehicle in the platoon contains nonlinear features generated from the powertrain and the motion of such vehicle could be described as:

$$\begin{bmatrix} \dot{s}_n \\ \dot{v}_n \\ \dot{a}_n \end{bmatrix} = \begin{bmatrix} v_n(k) \\ -\frac{C_{n,D}\rho_n A_n v_n^2(k)}{2m} - g(\mu \cos(\theta) + \sin(\theta)) + a_n(k) \\ \frac{1}{T}(u_n(k) - a_n(k)) \end{bmatrix} \quad (12)$$

where $\frac{1}{T}(u_n(k) - a_n(k))$ represents the response lag of the actuator and T is time constant based on the powertrain characteristic of the vehicle. $u_n(k)$ is the control input following the acceleration $a_n(k)$ at time point k . Considering the longitudinal dynamics above and energy variation as formula (10), the state vector is described as $\dot{x}_n(k) = [\dot{s}_n \quad \dot{v}_n \quad \dot{a}_n \quad \dot{SOC}_n]^T \in \mathbb{R}^4 Z$, where

and $\dot{x}_n(k) = f_n(x_n(k), u_n(k))$ is showed as:

$$\begin{bmatrix} v_n(k) \\ -\frac{C_{n,D}\rho_n A_n v_n^2(k)}{2m} - g(\mu \cos(\theta) + \sin(\theta)) + a_n(k) \\ \frac{1}{T}(u_n(k) - a_n(k)) \\ -(V_{OC}(k) + V_s(k)) - \sqrt{(V_{OC}(k) + V_s(k))^2 - 4R_e(k)T_{n,x}(k)\omega_{n,x}(k)\eta_m(k)\eta_b(k)^{-\text{sgn}(T_m(k))}} \\ 2R_e(k)Q_{MAX} \end{bmatrix} \quad (14)$$

Hence, the discrete-time dynamic could be displayed as

$$\begin{aligned} x_n(k+1) &= f(x_n(k), u_n(k)), k \geq 0 \\ y_{n,c}(k+1) &= g_{n,c}(x_n(k), u_n(k)) \end{aligned} \quad (15)$$

According to the theoretical basis of model predictive control that the dynamic behavior in the time domain of $[k, k+N_p]$ is

predicted at the current time point k . In this paper, the prediction time domain is $N_p = 5$, and the control time domain is $N_u = 3$, which satisfies $N_u \leq N_p$. After N_u steps, the control input remains unchanged i.e. $u_n(k+N_u-1) = u_n(k+N_u) \dots = u(k+N_p-1)$, and the predictive output equation at time point k is defined as

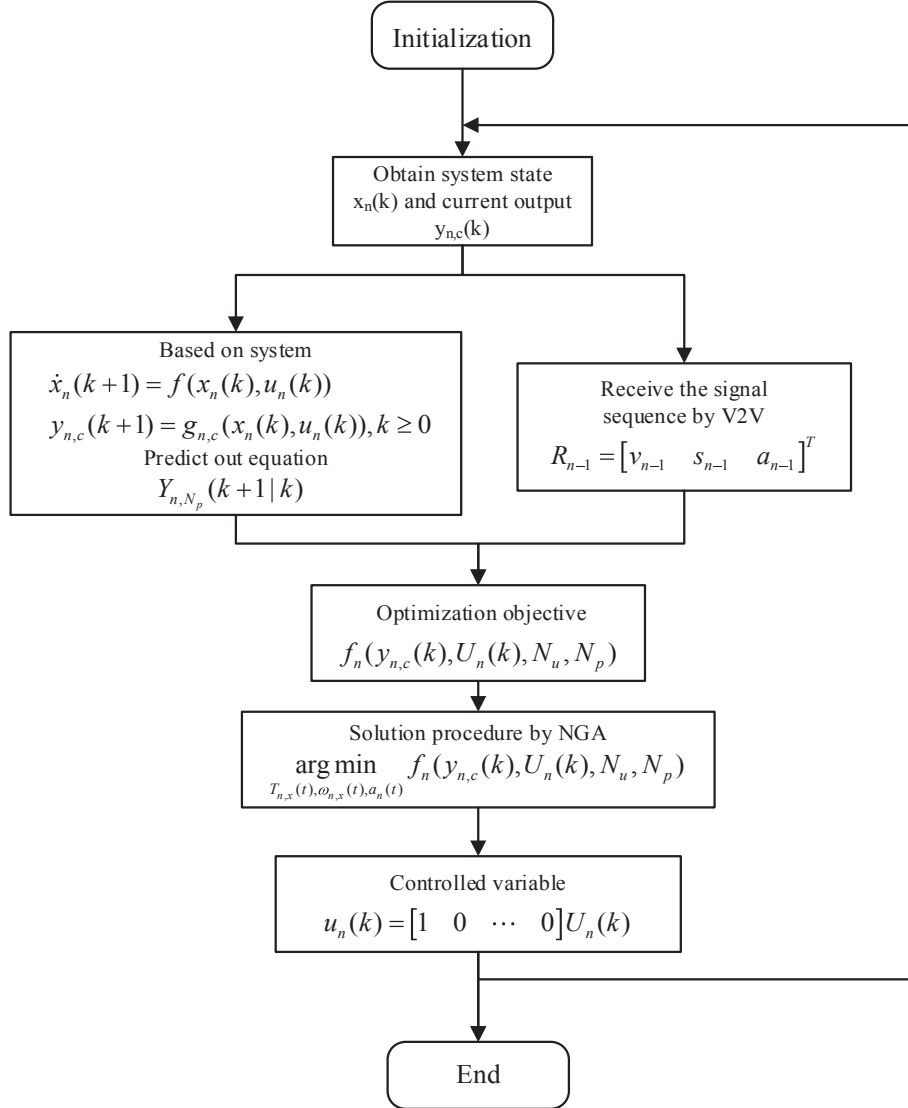


Fig. 3. Structure of controller design.

$$Y_{n,N_p}(k+1|k) \triangleq \begin{bmatrix} y_{n,c}(k+1|k) \\ y_{n,c}(k+2|k) \\ \vdots \\ y_{n,c}(k+N_p|k) \end{bmatrix} \quad (16)$$

likewise, the optimal control input sequence $U_n(k)$ at time k is defined as:

$$U_n(k) \triangleq \begin{bmatrix} u_n(k) \\ u_n(k+1) \\ \vdots \\ u_n(k+N_u-1) \end{bmatrix} \quad (17)$$

Based on principles and theories of model predictive control, the prediction equation of controlled output in N_p steps at time k can be deduced as follows:

$$\begin{aligned} y_{n,c}(k+1|k) &= g_{n,c}(x_n(k+1), u_n(k+1)) \\ &= g_{n,c}(f(x_n(k), u_n(k)), u_n(k+1)) \\ y_{n,c}(k+2|k) &= g_{n,c}(x_n(k+2), u_n(k+2)) \\ &= g_{n,c}(f(x_n(k+1), u_n(k+1)), u_n(k+2)) \\ &= g_{n,c}(f(f(x_n(k), u_n(k)), u_n(k+1)), u_n(k+2)) \\ &\vdots \\ y_{n,c}(k+N_p|k) &= g_{n,c}(x_n(k), u_n(k), u_n(k+1), \dots, u_n(k+N_u-1)) \end{aligned} \quad (18)$$

The reference input sequence is defined as the signal series $R_{n-1} = [v_{n-1} \ s_{n-1} \ a_{n-1}]^T$ delivered by the head and preceding vehicles based on the communication topology LPF:

$$R_{n-1}(k+1) = \begin{bmatrix} R_{n-1}^{sp}(k+1) \\ R_{n-1}^{sp}(k+2) \\ \vdots \\ R_{n-1}^{sp}(k+N_p) \end{bmatrix} \quad (19)$$

In this algorithm, the cost function is described to predict the preceding dynamics of the system, which is shown as:

$$f_n = \sum_{t=k}^{k+T_p} \frac{w_1(|v_{n-1}(k) - v_n(k)|\delta t) + w_2(\delta h(k)\delta t) + w_3(\delta q_n(k)\delta t)}{s_n(k+T_p) - s_n(k)} \quad (20)$$

where, $\delta q_n(k) = q_n(k+1) - q_n(k)$

The cost function f_n is the combined evaluation criteria of vehicle n related to the parameter of velocity, headway gap and energy consumption with weight assignment in predictive horizon T_p . Weight w_1 is assigned to the actual difference of the preceding and following vehicle, while weight w_2 makes effect to the headway gap deviation and weight w_3 concerns on the energy consumption of the following vehicle.

The energy-saving strategy of string stable vehicle platoon for each following vehicle n can be regarded as the minimization problem of cost function $f_n(y_{n,c}(k), U_n(k), N_u, N_p)$, which is defined as [35]:

$$U_n(t) = \underset{T_{n,x}(t), \omega_{n,x}(t), a_n(t)}{\operatorname{argmin}} f_n(y_{n,c}(k), U_n(k), N_u, N_p) \quad (21)$$

Table 2
Simulation parameters.

Parameters	Values
$C_{n,D}$	0.3350
ρ_n	1.2
A_n	2
m	977
g	9.81
μ	0.009
τ_h	0.6
l_0	2.5
r_0	10
$J_{n,x}$	1.2
g_n	3.92
r_w	0.282
L_n	1.89
H_n	0.5
$V_{OC}(k)$	500
$V_s(k)$	2.5
$R_s(k)$	0.07
$R_e(k)$	0.03
Q_{MAX}	60
T_p	10s
v_{min}	0
v_{max}	35
δh_{min}	-3
δh_{max}	3
SOC_{min}	0.2
SOC_{max}	0.8
$T_{n,xmax}$	240
$\omega_{n,xmax}$	8000
a_{nmin}	-3
a_{nmax}	3

$$\left\{ \begin{array}{l} v_{min} \leq v_n(k) \leq v_{max} \\ v_{min} \leq v_{n-1}(k) \leq v_{max} \\ \delta h_{min} \leq \delta h(k) \leq \delta h_{max} \\ SOC_{min} \leq SOC(k) \leq SOC_{max} \\ \max\{T_{n,xmin}, -\mu F_{r,x}(k)r_w\} \leq T_{n,x}(k) \leq \min\{T_{n,xmax}, \mu F_{r,x}(k)r_w\} \\ \omega_{n,xmin} \leq \omega_{n,x}(k) \leq \omega_{n,xmax} \\ a_{nmin} \leq a_n(k) \leq a_{nmax} \end{array} \right.$$

where each vehicle needs to maintain the velocity between the speed thresholds v_{min} and v_{max} . The headway gap deviation is inappropriate for intensive fluctuation (refers to δh_{min} and δh_{max}). Considering the overcharge and over discharge protection of the battery pack, the inferior limit SOC_{min} is set to 0.2 while the upper limit SOC_{max} is set to 0.8. To improve the operation stability of driving, the traction torque should be maintained under the $\min\{T_{n,xmax}, \mu F_{r,x}(k)r_w\}$ meaning that actual traction force is provided by the ground friction and needs to be less than $\mu F_{r,x}(k)$ when maximum traction torque $T_{n,xmax}$ is under the permission. Otherwise, $T_{n,xmax}$ is the only condition need to be considered. Similar as the torque constraint of the braking process. $\omega_{n,xmin}$ and $\omega_{n,xmax}$ are the minimum and maximum rotational speed of the motor x of the vehicle n . Furthermore, the value of the acceleration $a_n(k)$ is one of key factor affecting the riding comfortability which is emphatically controlled in the range of lower acceleration a_{nmin} and upper acceleration a_{nmax} in case of over fluctuating. As the nonlinear MPC cannot directly derive analytic solutions, the Numerical Algorithms Group (NAG) toolbox was employed for the solving process to obtain the control input sequence. The first element $u_n(k)$ of the obtained control sequence $U_n(k)$ was obtained and applied to the system. The flow chart of controller design is shown in Fig. 3.

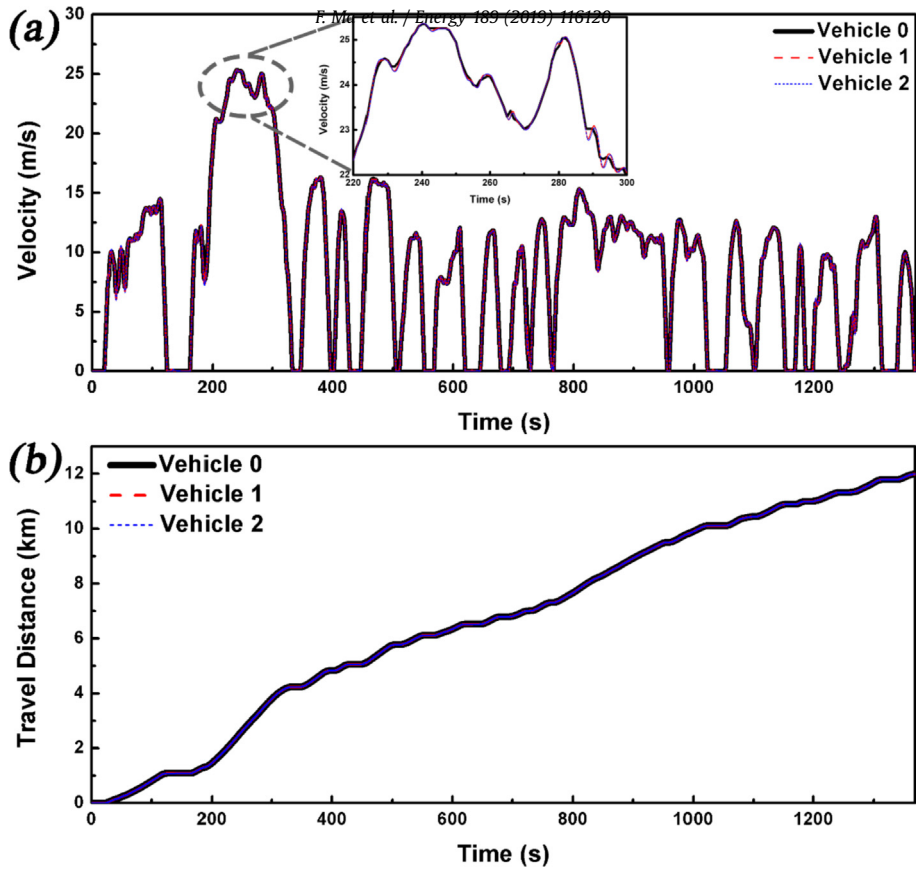


Fig. 4. (a)The following performance (insert is the detailed following description of the platoon) and (b) travel distance of vehicle platoon under full UDDS drive cycle using proposed NMPC strategy.

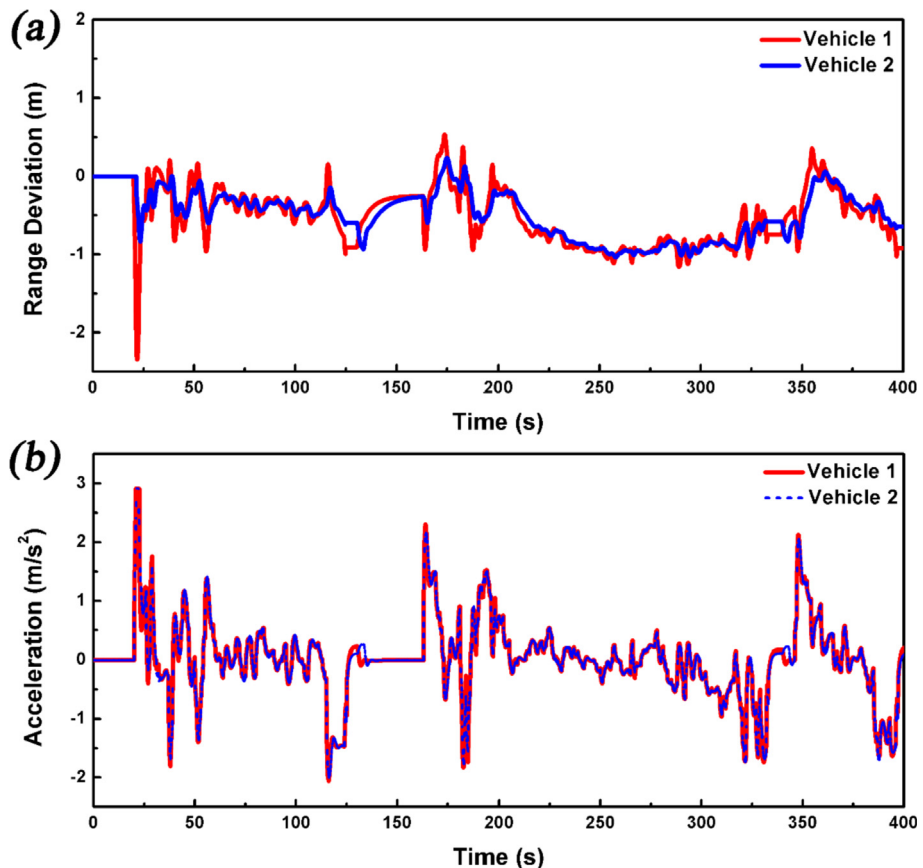


Fig. 5. (a) Range deviation and (b) acceleration of the following vehicles of the platoon under UDDS driving cycle in the first 400 s.

4. Performance evaluation

As is known, the precondition of energy-saving property of the platoon is the efficient driving and string stability. Therefore, the factors in the cost function include vehicle velocity, range deviation and energy consumption of the platoon are considered in proposed NMPC strategy. The selected parameters for simulation are listed in Table 2.

4.1. Result for the urban drive cycle

To verify the performance of the energy-saving NMPC strategy applying to the connected autonomous vehicle platoon, the fuel economy testing drive cycle referred to UDDS flow condition is considered. Here, the leading vehicle of the platoon is denominated as vehicle 0, which completely follows the speed profile of UDDS drive cycle. While the following vehicles referred to vehicle 1 and vehicle 2 will track vehicle 0 using the proposed control strategy. Fig. 4a shows the following performance of vehicle platoon and it can be seen that the following vehicles display superior tracking ability with minority fluctuation when vehicle 0 happens to accelerate or deceleration. The fluctuation appears to the peak and valley of the speed profile due to the existing response process of the controller. Moreover, there is commonly happened to be a little time delay and overshoot in the response process against the controlled object. The insert figure is the detailed following

description of the platoon, which reveals the similar tracking accuracy of both vehicle 1 and vehicle 2. Compared to the curve of vehicle 1, that of vehicle 2 comes out an inconspicuous offset along time (positive direction of X-axis), which is caused by a little slower response time affected by V2V communication topology that the following vehicle receive the signal from both of the leading vehicle and preceding vehicle [36]. Another way to evaluate the travel distance which is shown in Fig. 4b. The curves of the vehicle 1 and vehicle 2 coincide with that of vehicle 0 and rarely appear obvious divariation during the whole drive cycle. That is all the vehicle travel almost the same distance at every time point k . At the end of the drive cycle all the three vehicles drives totally about 11.9902 km (vehicle 0), 11.9897 km (vehicle 1) and 11.9893 km (vehicle 2) respectively, which illustrates the travel distance error is less than 1 m after the nearly 12 km traveling. Above these, it can be said that the platoon exhibits an excellent following performance at the macro level.

To comprehensively investigate the string performance, the detailed description in the first 400 s part of UDDS cycle can be more intuitionistic to reveal the features of the two following vehicles. The range deviation represents the difference of desired headway gap and current headway gap, and Fig. 5a displays that of vehicle 1 and vehicle 2. The fluctuation range is less than 3 m during the whole process and even less than 1.5 m if without regard to vehicle starting procedure. As for the vehicle 1, the controller

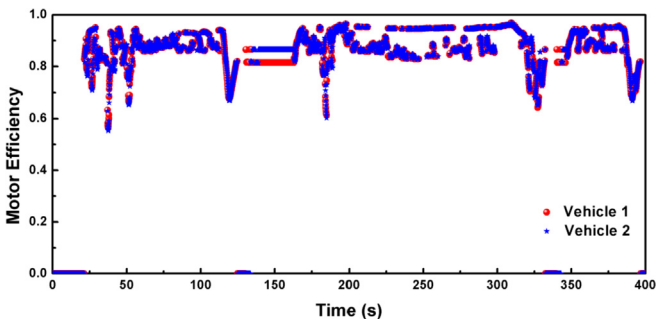


Fig. 6. Motor efficiency of the following vehicles of the platoon under UDDS driving cycle in the first 400 s.

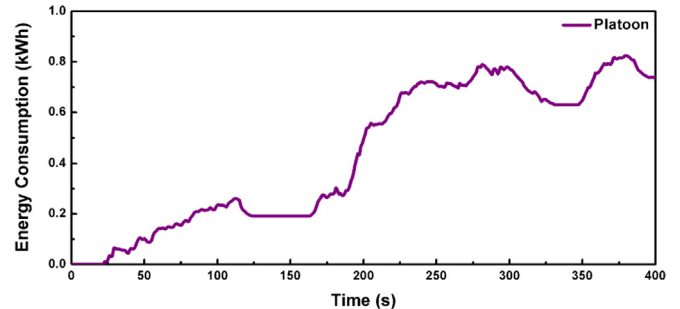


Fig. 8. Total energy consumption of the platoon under UDDS driving cycle in the first 400 s.

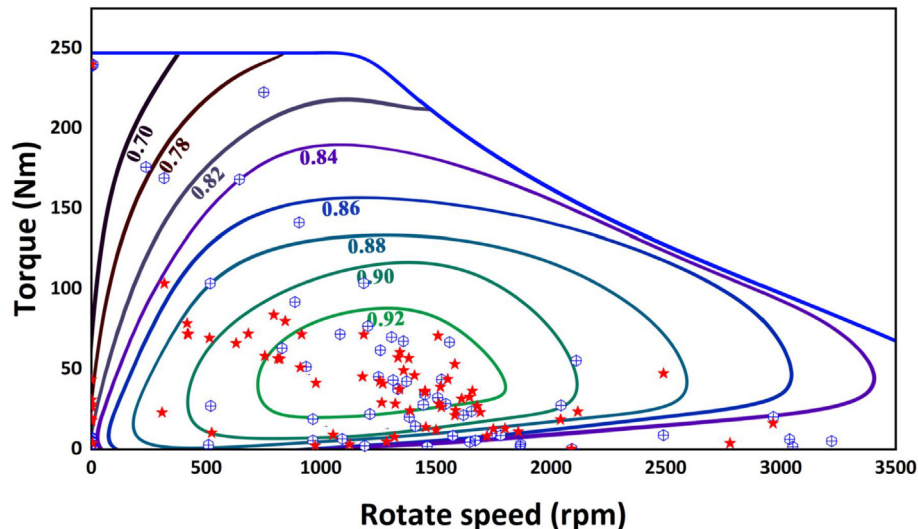


Fig. 7. Comparison of motor operating point distribution with (symbol: red star) and without (symbol: blue cycle) consideration of energy consumption in cost function of the NMPC scheme.

owns response time at the starting process that the vehicle accelerates from a complete stop statue, resulting a relatively large range deviation occurs. While the vehicle 2 also exists the same situation. However, vehicle 2 receipts signal both from the leading vehicle and the preceding vehicle due to the cooperative V2V communication, which makes the controller of vehicle 2 begin to operate when the vehicle 0 starts so that the intervehicle headway gap between vehicle 1 and 2 maintains in a small range. Further, it is obviously that the range deviation of vehicle 2 is smaller than that of vehicle 1, indicating the fluctuation of the following vehicle in the platoon is convergent [37]. As is shown in Fig. 5b, the acceleration curves of the two following vehicles range from -2 m/s^2 and 3 m/s^2 , and the resulting acceleration is beneficial for energy saving and driving comfort of the platoon [28]. Compared the two curves, both of them own the similar tendency and the peak values of the blue curve is slightly less than the red one during the whole process, which is also an evidence exhibiting the superior following performance of the CAV platoon [38].

Excellent string stability of the platoon could decrease the error transmission while the leading vehicle appears the parameter fluctuation such as velocity. It means that the following vehicles perform more smoothly compared to driving without string stability. As known, aggressive driving such as rapid acceleration and deacceleration could make the motor operating points drifting away from the high-efficiency area and generate more energy loss in energy conversion process, which is regarded as one of the key factors for the energy consumption. Therefore, the relative smooth driving with string stability is beneficial for energy-saving. Energy economy has strong relationship with the motor efficiency. From

Fig. 6, the operation points of both following vehicles reveal the similar distribution by the following property of the platoon and majority of them concentrate in the high efficiency area where

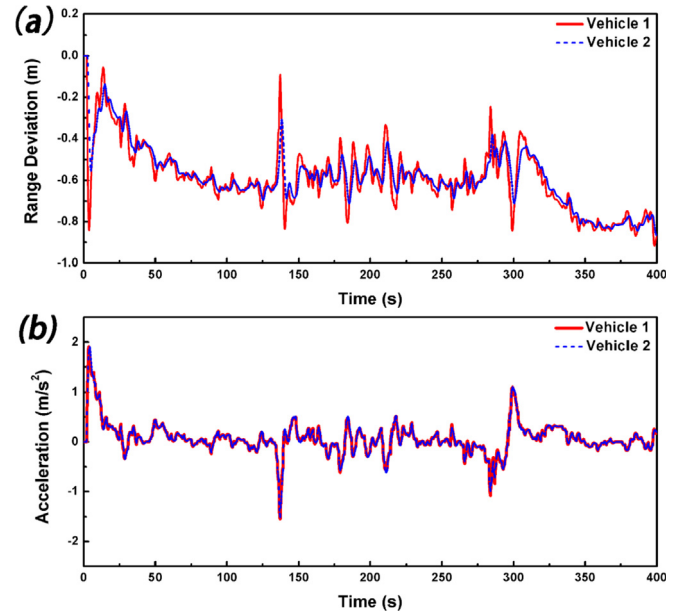


Fig. 10. (a) Range deviation, (b) acceleration and SOC variation of the following vehicles of the platoon under HWFET driving cycle in the first 400 s.

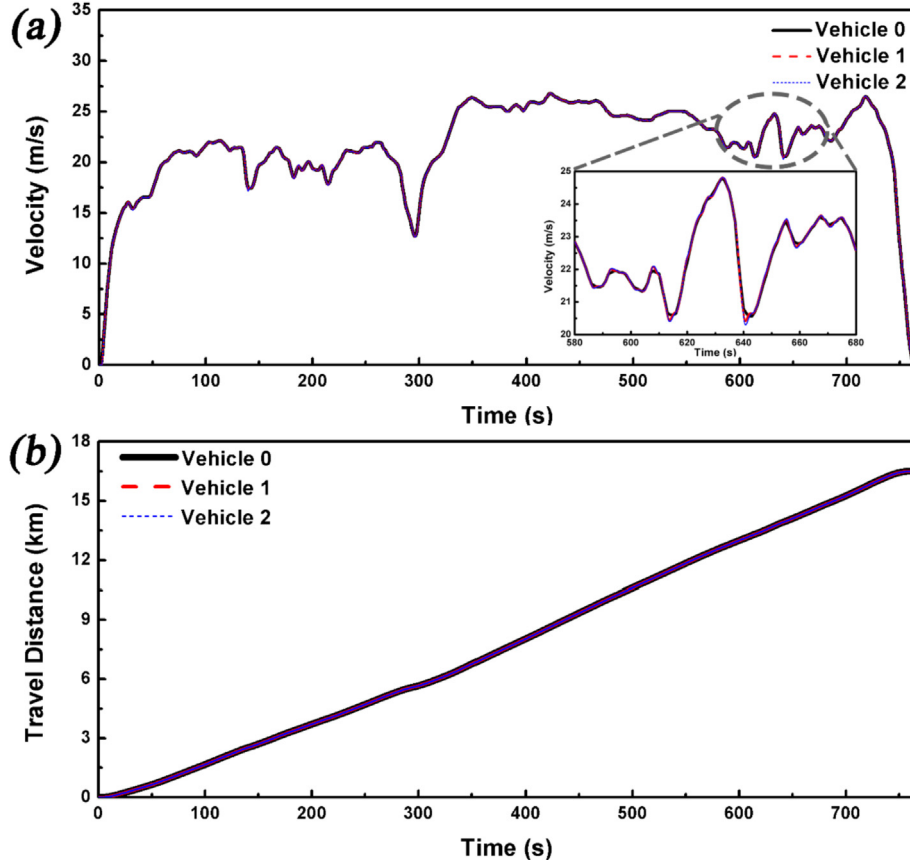


Fig. 9. (a) The following performance (insert is the detailed following description of the platoon) and (b) travel distance of vehicle platoon under full HWFET drive cycle using proposed NMPC strategy.

represents less energy consumption. The operation points distributed in the efficiency region equaling to zero means the current vehicle in the stop condition and the motors do not rotate.

In order to further verify that the energy economy can be improved by considering the energy consumption in cost function of the controlled scheme, the motor operating point distribution with and without considering the energy consumption in the cost function was compared in Fig. 7. The red star represents the scheme considering energy consumption in the cost function while the blue cycle is the one without considering that. In the motor efficiency map, more red stars distribute in the high-efficiency region compared to blue cycles, illustrating the motor was optimized to exhibit better energy-saving potential.

In the actual application case, the vehicles could form homogeneous platoon consisted of the vehicle with the same parameters and heterogeneous platoon consisted of different vehicles with various properties. Therefore, the total energy consumption of the platoon and average energy consumption per vehicle attract more attention, which could reflect the energy-saving characteristics of whatever vehicle platoon. Fig. 8 shows total energy consumption of the platoon consisted of 3 investigating vehicles under UDDS driving cycle in the first 400 s. With the time goes by, the energy consumption of the platoon displays three variation situations. Except for the increasing processes represent the normal energy requirement, the decreasing parts come from deceleration with the braking energy recovery and the platform areas refer to the parking procedures of the vehicle platoon. After the first 400 s of the UDDS driving cycle, the total energy consumption of the platoon is 0.738 kWh including the pure consumed energy and regenerative energy corresponding to the acceleration phase and decelerating phase.

4.2. Results for the highway drive cycle

To further evaluate the overall property of the vehicle platoon included following performance and energy-saving characteristic in high speed driving, the dedicated test flow condition for energy

consumption named Highway Fuel Economy Test (HWFET) drive cycle is conducted and assigned to the leading vehicle as the ve-

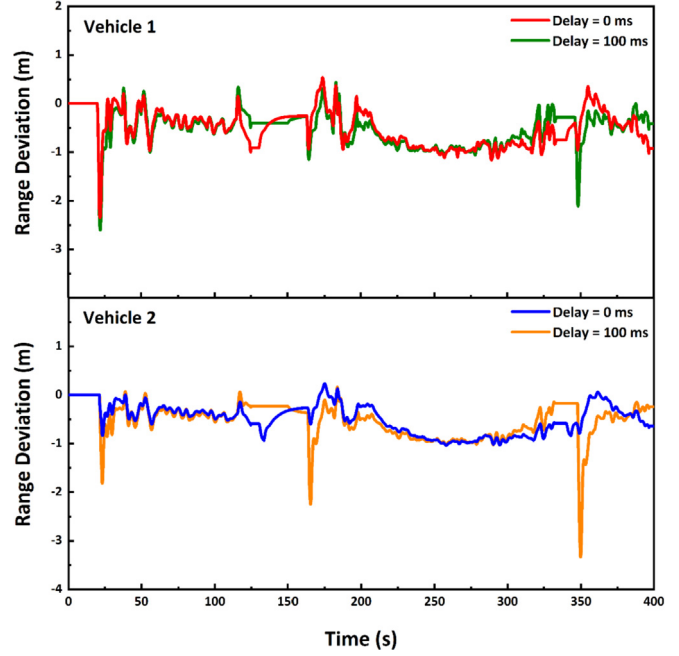


Fig. 12. Comparation of range deviation of Vehicle 1 and Vehicle 2 under the ideal communication condition and real condition with time delay of 100 ms.

locity profile. It can be found in Fig. 9a that the following vehicle 1 and vehicle 2 exhibit excellent tracking ability to follow the speed trajectory of the leading vehicle 0 using proposed NMPC strategy during the whole process of HWFET drive cycle. The characteristic of the highway driving is that the speed range mainly distributes in the high region without plenty of dramatical fluctuation, which is more suitable for the NMPC controller. And as the detailed



Fig. 11. LTE-V communication device of DTVL3100-OBU.

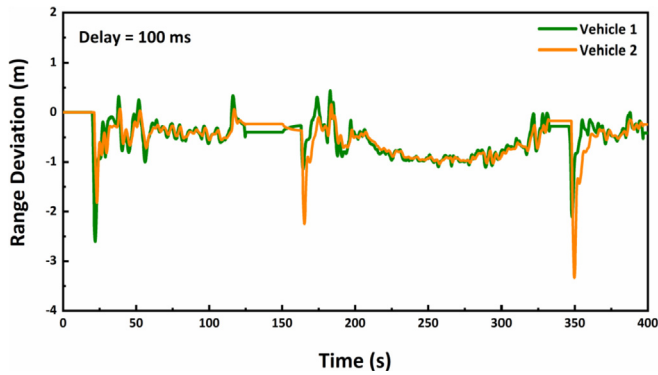


Fig. 13. Range Deviation of Vehicle 1 and Vehicle 2 with communication time delay of 100 ms.

description shown in the insert graph of Fig. 9a, the control effect of the following vehicles is relatively steady in the area where jerk (changing rate of acceleration) of the leading vehicle is small, while moderate overshoots of the controller exist in the region where jerk is high. The travel distance of the vehicle platoon is indicated in Fig. 9b and coincident curves reveal the desired following ability. At the end of the HWFET drive cycle, the total mileage of three vehicles is 16.5065 km, 16.5056 km and 16.5046 km respectively.

Compared with urban driving in UDDS flow condition, the platoon also shows excellent performance in highway driving under HWFET driving, which can be confirmed in Fig. 10a. The overall range deviation of the both vehicles is no more than 0.9 m which is

less than that in urban driving, indicating the platoon owns splendid following ability in high speed driving. Likewise, the acceleration of the both vehicles in such drive cycle provided in Fig. 10b distributes in the range of -2 m/s^2 and 2 m/s^2 with small and relative steady fluctuation, which improves the energy economy and drive comfort fluctuation [39]. Through the above discussion, the vehicle platoon demonstrates satisfactory comprehensive performance in high speed driving condition.

4.3. Results for driving cycle with consideration of time delay

The time delay is an unavoidable feature existing in the real devices influencing the effectiveness of V2V communication. In the proposed scheme, the parameters of communication device were chosen according to DTVL3100-OBU (Fig. 11) fabricated by Datang Telecom Technology & Industry Group as the V2V devices which exhibit the time delay of about 50 ms from its technical specification. Herein, in the simulation, the frequency of the system was 0.1 s communication delay was set as 100 ms.

The first 400 s of UDDS driving cycle was employed to investigate the vehicle following performance of Vehicle 1 and Vehicle 2 with time delay. Fig. 12 illustrates that the vehicle following performance was influenced by the information delay especially in the vehicle start-up stage of 25 s, 165 s and 350 s. The following vehicle does not receive the signals transmitted by the preceding vehicle at the time point that preceding vehicle begins to start up due to the time delay, resulting in generating the intervehicle distance in this process. However, the proposed controller could quickly adjust the following errors to a stable status when the vehicles begin to drive.

Fig. 13 exhibits the range deviation of the following vehicles

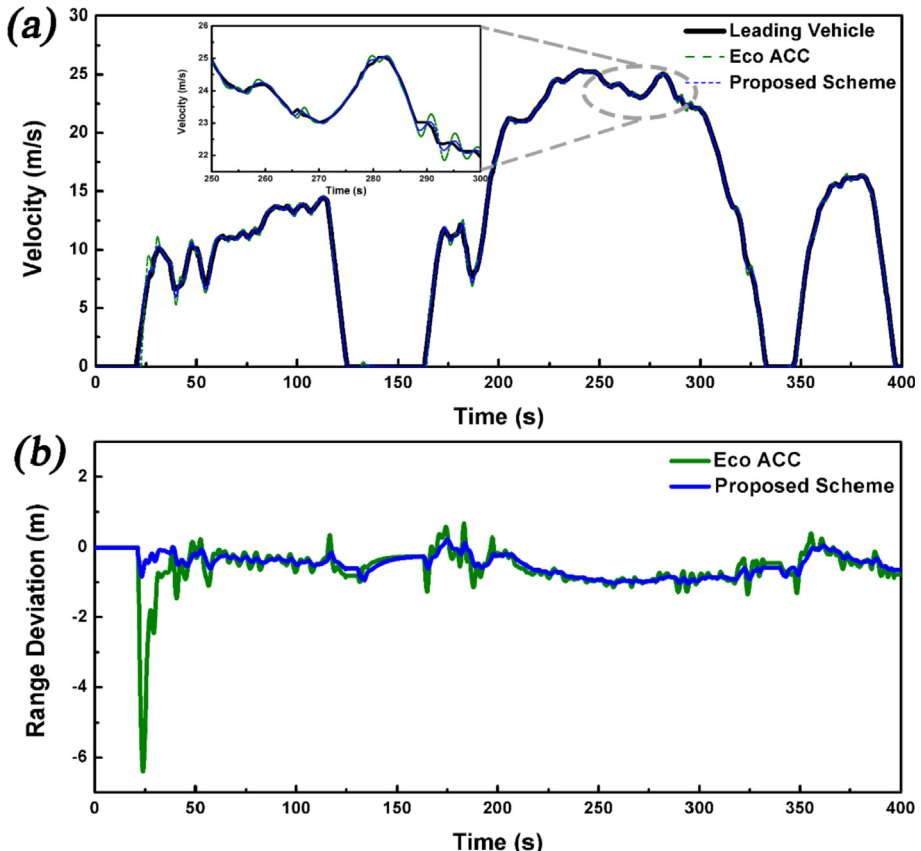


Fig. 14. Comparison of (a) the following performance (the insert is the detailed following description) and (b) range deviation of the following vehicle using eco ACC and proposed control strategy under UDDS drive cycle in the first 400 s.

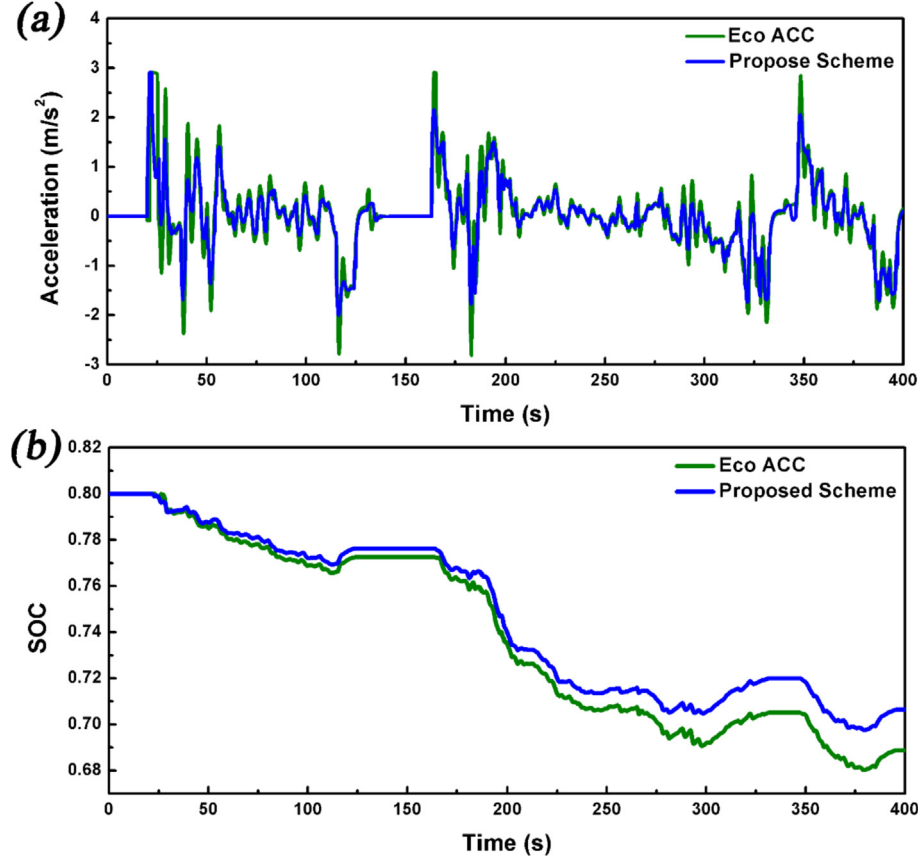


Fig. 15. Comparison of (a) acceleration and (b) SOC variation of the following vehicle using Eco ACC and proposed control strategy under urban drive cycle in the first 400s.

under the consideration of time delay. In the vehicle driving process especially cruising, the range deviation of each vehicle was less than 2 m, where the vehicle 2 is more stable than vehicle 1. While in the total 400s driving cycle, the maximum range deviation is still less than 4 m, which reveals the favorable vehicle following performance of the platoon.

5. Comparison with existing control strategy

It is meaningful to make a comparison with the existed controller. Therefore, the NMPC-based Eco ACC strategy proposed by Ref. [26] is investigated in simulation. The essential feature of this strategy is that the following vehicle obtain the decision-making acceleration to keep the headway gap with the preceding vehicle using the self-equipped sensors without cooperative communication. Moreover, the controller will adjust the torque and rotated speed in the high efficiency area of the motor map according to the desired acceleration. The Eco ACC in our manuscript possesses the same scheme as the proposed controller but for the input signals, i.e. the approach of signal acquisition is different.

Among the simulation result, the following performance of the current vehicle by Eco ACC and proposed control strategy under urban flow condition in the first 400 s. It is obvious in Fig. 14a that green dashed presents a slow response when the leading vehicle accelerates from stopping at the first 25 s, resulting the large range deviation (Fig. 14b) here while the following vehicle using proposed scheme has a quick response and avoid the dramatic variation with the desired headway gap using V2V communication. Moreover, the overshoot of Eco ACC controller is more serious when acceleration

and deceleration of the leading vehicle happen especially those sharply vary, which is observed in the insert graph of Fig. 14a. The more fluctuation and slow response make against the string stability and energy economy of the vehicle platoon. As discussed above, in the aspect of vehicle following, the proposed strategy owns a better performance compare to Eco ACC controller.

As for the acceleration variation presented in Fig. 15a, under the same vehicle following requirements the blue curve exhibits the fluctuation within a narrower range compared to the green one,

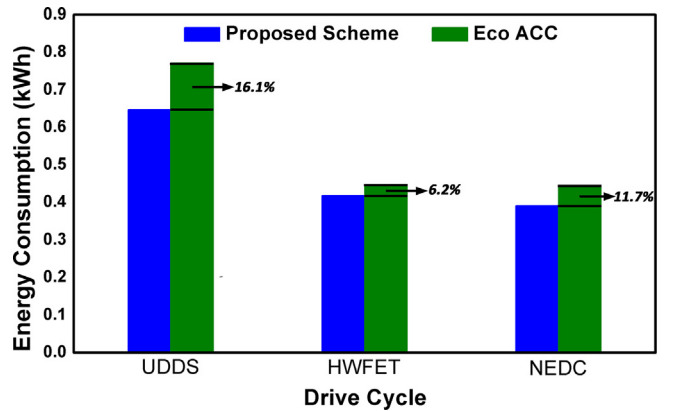


Fig. 16. Comparation of the energy-saving performance of the following vehicle using Eco ACC and proposed control strategy under full UDDS, HWFET and NEDC drive cycle.

suggesting that the velocity of the following vehicle using proposed NMPC strategy changes more smoothly which get benefits to improve the drive comfort as well as the energy economy [40]. Besides, the Eco ACC controller reaches the upper bound setting from -3 m/s^2 to 3 m/s^2 for multiple times, which also decrease its performance evaluation tradeoff. The energy-saving potential of the both strategies can be reflected by SOC which is the key parameter which could intuitively exhibit the comprehensive energy consumption of the fully electric vehicle. Fig. 15b shows SOC variation of the following vehicle implement Eco ACC and proposed control strategy under UDDS driving cycle in the first 400 s. The initial SOC value of the battery pack is set as 0.8, and the curves decrease when the vehicles proceed cruising and acceleration while SOC value of the following vehicle increases in some parts

due to regenerative braking energy in the decelerating process. Obviously, the SOC of the Eco ACC displays a rapid downward tendency compared to that of proposed scheme and it decreases more faster as time goes. At the point of 400 s, the SOC value of proposed scheme still remain at 0.706 while the other is already 0.688, demonstrating the advantageous energy economy of the proposed controller.

The standard fuel economy drive cycle of UDDS, HWFET and NEDC can convincingly demonstrate the energy consumption level of the vehicle. As is shown in Fig. 16, the energy-saving performance of the following vehicle using proposed control strategy is compared with that utilizing the Eco ACC benchmark under the above full drive cycle. The proposed scheme presents less average energy consumption of the following vehicle of 0.6470 kWh,

Table 3
Comparisons of the simulation results under the different drive cycle.

Drive cycle	Methodology	Energy consumption	Performance improvement
UDDS	Proposed NMPC	0.6470 kWh	16.1%
	Eco ACC	0.7716 kWh	Base
HWFET	Proposed NMPC	0.4183 kWh	6.2%
	Eco ACC	0.4461 kWh	Base
NEDC	Proposed NMPC	0.3914 kWh	11.7%
	Eco ACC	0.4432 kWh	Base

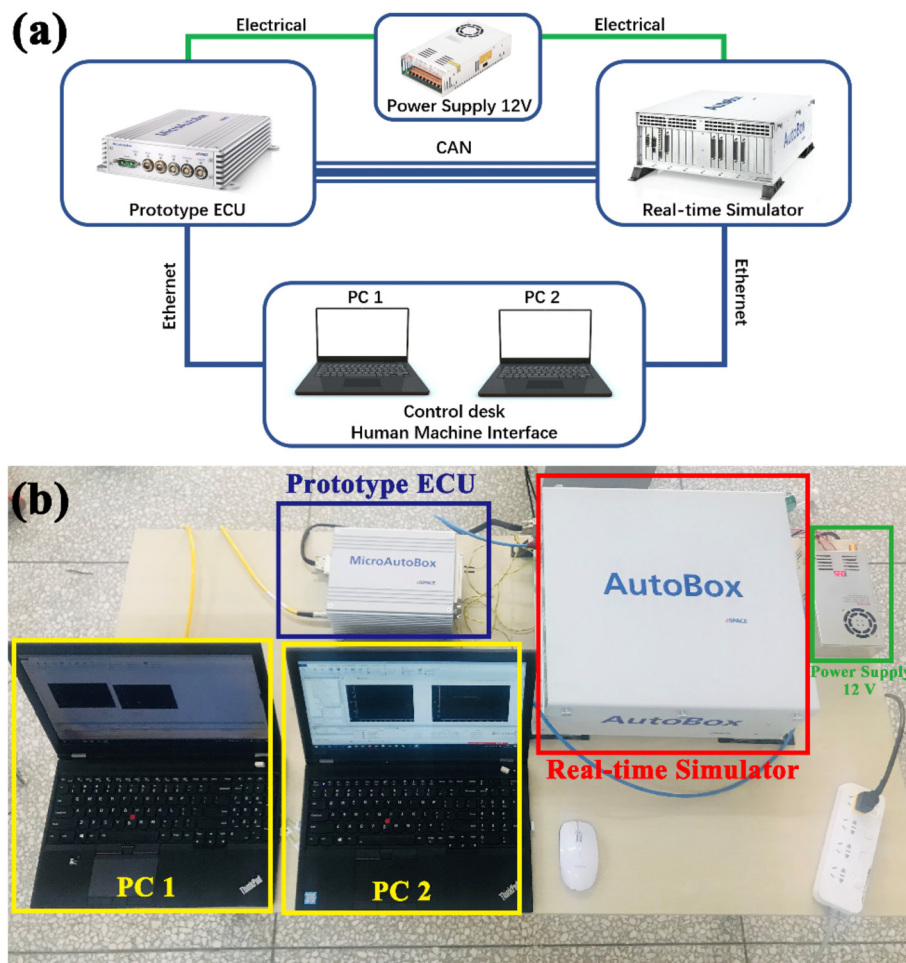


Fig. 17. (a) Schematic and (b) the actual arrangement of the HIL experiment.

0.4183 kWh and 0.3914 kWh as opposed to Eco ACC controller of 0.7716 kWh, 0.4461 kWh and 0.4432 kWh under UDDS, HWFET and NEDC flow condition, respectively. Moreover, in the case of HWFET drive cycle, the energy-saving performance of NMPC controller is about 6.2% relative to benchmark which is a bit too less than that under UDDS of 16.7% and NEDC of 11.7%. And this can be explained that the mentioned two strategy have a good performance in the area of steady velocity variation while NMPC controller performs better in the area of drastic acceleration and deceleration. Coincidentally, most of HWFET drive cycle is high speed level with less acceleration and deceleration which could help to operate the in-wheel motors in the high efficiency region, resulting in the little difference of the energy-saving potential of both two controllers. The detailed comparisons of the simulation results under the three presented drive cycles are provided in [Table 3](#).

6. Real-time implementation

To further verify the model accuracy of the simulation model, the real-time implementation as hardware-in-loop (HIL) was carried out [\[41\]](#). HIL provides an effective platform by adding the complexity of the plant under control to the test platform where

the communication issues and computing resource allocation are considered. Hence, the obtained results are more convincing than the software-level simulation. In the experiments, the HIL arrangement ([Fig. 17](#)) mainly consisted of four components as human-machine interface, prototype ECU, real-time simulator and 12 V DC power supply. The proposed control scheme was loaded from PC 1 to the prototype ECU while the controlled plant was read by real-time simulator from PC 2 with the ethernet communication. The prototype ECU delivers the control instruction to real-time simulator through Controller Area Network (CAN). The results can be collected from the human-machine interface software “dSPACE Control Desk 6.4”. The hardware sources are as follows: 1) Prototype ECU is derived from dSPACE/MicroAutoBox II (DS-1401); 2) Real-time simulator is provided as dSPACE/AutoBox (DS-1007); 3) PC 1 and PC 2 are Lenovo ThinkPad P52; 3) 12 V DC power supply is manufactured as Senqi KT-500-48.

From the real-time implementation results in [Fig. 18](#), the velocity following performance and range deviation of both following vehicles exhibit little bigger amplitude and more fluctuation compared to the simulation results, which demonstrates the influence caused by communication delay of CAN-BUS, response speed of controller, computational efficiency and disturbance of

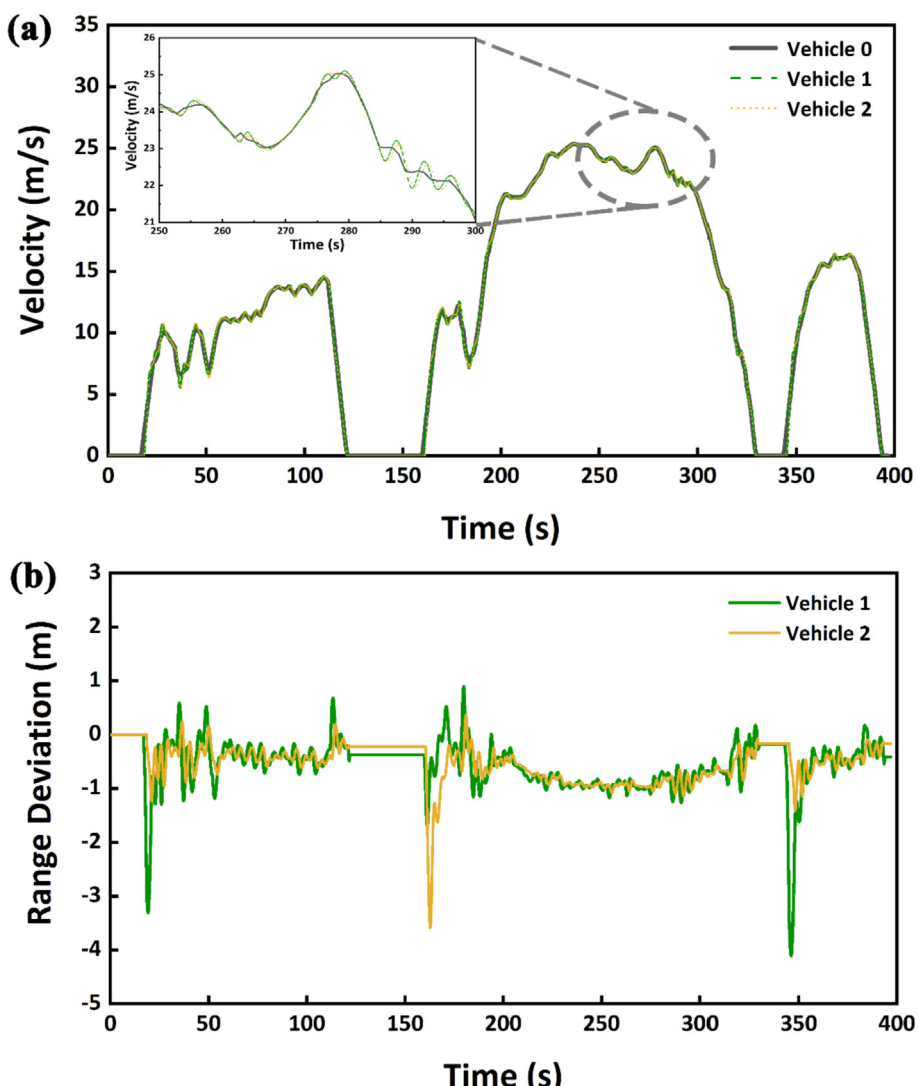


Fig. 18. (a) Velocity variation and (b) range deviation of following vehicles driven by the controller in HIL experiments.

external environment to the signals. The effectiveness of proposed scheme was validated and the experimental outcomes are favorable for the real-time implementation even future application.

7. Conclusions

This paper proposed eCACC strategy using NMPC method for a CAV platoon consisted of three electric vehicles to minimize the energy consumption under the V2V topological communication structure of LPF. The scheme largely improves the car-following performance in common speed driving condition with smaller range deviation even considering communication time delay, which was also verified by the real-time implementation. In addition, the simulation results present a satisfied energy-saving potential for a 977 kg mini electric vehicle under UDDS, HWFET, NEDC drive cycle with energy efficiency improvement of 16.1%, 6.2%, 11.7% respectively compared to the existing Eco ACC controller. Except for the energy-saving potential, the drive comfort and string ability of the proposed scheme are in a desirable level. However, to accelerate the further application in daily scenario, the future works will be conducted focusing on following two aspects. The first one is to investigate the energy economy property under the various topological communication structure and the second is to improve the proposed strategy considering the lateral control such as splitting and merging under the complicated scenarios.

Acknowledgments

This work is supported by the Jilin Province Key Technology and Development Program (No. 20190302077GX) and National Key Technologies R&D Program of China during the 13th Five-Year Plan Period (No. 2017YFC0601604).

References

- [1] Xu Y, Li H, Liu H, Rodgers MO, Guensler RL. Eco-driving for transit: an effective strategy to conserve fuel and emissions. *Appl Energy* 2017;194:784–97.
- [2] Guo G, Wang Q. Fuel-efficient en route speed planning and tracking control of truck platoons. *IEEE Trans Intell Transp Syst* 2018;14(8):1–13.
- [3] Huang Y, Ng ECY, Zhou JL, Surawski NC, Chan EFC, Hong G. Eco-driving technology for sustainable road transport: a review. *Renew Sustain Energy Rev* 2018;93:596–609.
- [4] He W, Wang S. Thermolectric performance optimization when considering engine power loss caused by back pressure applied to engine exhaust waste heat recovery. *Energy* 2017;133:584–92.
- [5] Yang Y, Xi Y, Li J, Wei G, Klyui NI, Han W. Flexible supercapacitors based on polyaniline arrays coated graphene aerogel electrodes. *Nanoscale Res Lett* 2017;12(1):394–403.
- [6] Adefarati T, Bansal RC. Reliability and economic assessment of a microgrid power system with the integration of renewable energy resources. *Appl Energy* 2017;206:911–33.
- [7] Guo L, Gao B, Gao Y, Chen H. Optimal energy management for HEVs in eco-driving applications using Bi-level MPC. *IEEE Trans Intell Transp Syst* 2017;18(8):2153–62.
- [8] Jiang H, Hu J, An S, Wang M, Park BB. Eco approaching at an isolated signalized intersection under partially connected and automated vehicles environment. *Transp Res C Emerg Technol* 2017;79:290–307.
- [9] Qiu C, Wang G, Meng M, Shen Y. A novel control strategy of regenerative braking system for electric vehicles under safety critical driving situations. *Energy* 2018;149:329–40.
- [10] Zhang S, Luo Y, Wang J, Wang X, Li K. Predictive energy management strategy for fully electric vehicles based on preceding vehicle movement. *IEEE Trans Intell Transp Syst* 2017;18(11):3049–60.
- [11] Juan A, Mendez C, Faulin J, de Armas J, Grasman S. Electric vehicles in logistics and transportation: a survey on emerging environmental, strategic, and operational challenges. *Energies* 2016;9(2):86–107.
- [12] Luo Y, Chen T, Zhang S, Li K. Intelligent hybrid electric vehicle ACC with co-ordinated control of tracking ability, fuel economy, and ride comfort. *IEEE Trans Intell Transp Syst* 2015;16(4):2303–8.
- [13] Qi X, Wu G, Hao P, Boriboonsomsin K, Barth MJ. Integrated-connected eco-driving system for PHEVs with Co-optimization of vehicle dynamics and powertrain operations. *IEEE Trans Intell Veh* 2017;2(1):2–13.
- [14] Li SE, Li R, Wang J, Hu X, Cheng B, Li K. Stabilizing periodic control of automated vehicle platoon with minimized fuel consumption. *IEEE Trans Transp Electrif* 2017;3(1):259–71.
- [15] Liu T, Hu X, Li SE, Cao D. Reinforcement learning optimized look-ahead energy management of a parallel hybrid electric vehicle. *IEEE/ASME Trans Mechatronics* 2017;22(4):1497–507.
- [16] Li SE, Xu S, Huang X, Cheng B, Peng H. Eco-departure of connected vehicles with V2X communication at signalized intersections. *IEEE Trans Veh Technol* 2015;64(12):5439–50.
- [17] Talavera E, Díaz-Alvarez A, Jiménez F, Narango J. Impact on congestion and fuel consumption of a cooperative adaptive cruise control system with lane-level position estimation. *Energies* 2018;11(1):194–211.
- [18] Cui L, Jiang HF, Park BB, Byon YJ, Hu J. Impact of automated vehicle eco-approach on human-driven vehicles. *Ieee Access* 2018;6:62128–35.
- [19] Fredette D, Ozguner U. Dynamic eco-driving's fuel saving potential in traffic: multi-vehicle simulation study comparing three representative methods. *IEEE Trans Intell Transp Syst* 2018;19(9):2871–80.
- [20] Thibault L, De Nunzio G, Sciarretta A. A unified approach for electric vehicles range maximization via eco-routing, eco-driving, and energy consumption prediction. *IEEE Trans Intell Vehi* 2018;3(4):463–76.
- [21] Zheng Y, Li SE, Li K, Borrelli F, Hedrick JK. Distributed model predictive control for heterogeneous vehicle platoons under unidirectional topologies. *IEEE Trans Control Syst Technol* 2017;25(3):899–910.
- [22] Chen W, Liu Y. Gap-based automated vehicular speed guidance towards eco-driving at an unsignalized intersection. *Transp B Trans Dyn* 2017;1:22.
- [23] Lei F, Bai Y, Zhu W, Liu J. A novel approach for electric powertrain optimization considering vehicle power performance, energy consumption and ride comfort. *Energy* 2019;167:1040–50.
- [24] Wang H, Peng P, Huang Y, et al. Model predictive control-based eco-driving strategy for CAV. *IET Intell Transp Syst* 2019;13(2):323–9.
- [25] Orosz G. Connected cruise control: modelling, delay effects, and nonlinear behaviour. *Veh Syst Dyn* 2016;54(8):1147–76.
- [26] Vajedi M, Azad NL. Ecological adaptive cruise controller for plug-in hybrid electric vehicles using nonlinear model predictive control. *IEEE Trans Intell Transp Syst* 2015;17(1):113–22.
- [27] Zheng Y, Li SE, Li K, Wang L. Stability margin improvement of vehicular platoon considering undirected topology and asymmetric control. *IEEE Trans Control Syst Technol* 2016;24(4):1253–65.
- [28] Hu X, Wang H, Tang X. Cyber-physical control for energy-saving vehicle following with connectivity. *IEEE Trans Ind Electron* 2017;64(11):8578–87.
- [29] Zhai C, Luo F, Liu Y. Cooperative look-ahead control of vehicle platoon for maximizing fuel efficiency under system constraints. *IEEE Access* 2018;6:37700–14.
- [30] Li L, Wang X, Song J. Fuel consumption optimization for smart hybrid electric vehicle during a car-following process. *Mech Syst Signal Process* 2017;87:17–29.
- [31] Xiong R, Duan Y, Cao J, Yu Q. Battery and ultracapacitor in-the-loop approach to validate a real-time power management method for an all-climate electric vehicle. *Appl Energy* 2018;217:153–65.
- [32] Chen Dj, Ahn S, Chitturi M, Noyce D. Truck platooning on uphill grades under cooperative adaptive cruise control (CACC). *Transp Res C Emerg Technol* 2018;94:50–66.
- [33] Flores C, Milanes V. Fractional-order-based ACC/CACC algorithm for improving string stability. *Transp Res C Emerg Technol* 2018;95:381–93.
- [34] Lee JH. Model predictive control: review of the three decades of development. *Int J Control Autom Syst* 2011;9(3):415–24.
- [35] Yu K, Xu X, Liang Q, Hu Z, Yang J, Guo Y, et al. Model predictive control for connected hybrid electric vehicles. *Math Probl Eng* 2015:1–15. 2015.
- [36] Tamilarasan S, Guvenic L. Impact of different desired velocity profiles and controller gains on convoy driveability of cooperative adaptive cruise control operated platoons. *SAE Int J Passeng Cars - Mech Syst* 2017;10(1):93–101.
- [37] Naus GJL, Vuugts RPA, Ploeg J, van de Molengraft MJG, Steinbuch M. String-stable CACC design and experimental validation: a frequency-domain approach. *IEEE Trans Veh Technol* 2010;59(9):4268–79.
- [38] Emirler MT, Guvenic L, Guvenic BA. Design and evaluation of robust cooperative adaptive cruise control systems in parameter space. *Int J Auto Tech-Kor.* 2018;19(2):359–67.
- [39] Wang H, Huang Y, Khajepour A, He H, Cao D. A novel energy management for hybrid off-road vehicles without future driving cycles as a priori. *Energy* 2017;133:929–40.
- [40] Kamal MAS, Mukai M, Murata J, Kawabe T. Ecological vehicle control on roads with up-down slopes. *IEEE Trans Intell Transp Syst* 2011;12(3):783–94.
- [41] Sakhdari B, Azad NL. Adaptive tube-based nonlinear MPC for economic autonomous cruise control of plug-in hybrid electric vehicles. *IEEE Trans Veh Technol* 2018;67(12):11390–401.